

ASME Letters in Dynamic Systems and Control Online journal at:

https://asmedigitalcollection.asme.org/lettersdynsys



Preston Fairchild²

Department of Electrical and Computer Engineering, Michigan State University, East Lansing, MI 48824 e-mail: fairch42@msu.edu

Noah Shephard

Department of Electrical and Computer Engineering, Michigan State University, East Lansing, MI 48824 e-mail: shepha12@msu.edu

Yu Mei

Department of Electrical and Computer Engineering, Michigan State University, East Lansing, MI 48824 e-mail: meiyu1@msu.edu

Xiaobo Tan

Department of Electrical and Computer Engineering, Michigan State University, East Lansing, MI 48824 e-mail: xbtan@egr.msu.edu

Semi-Physical Modeling of Soft Pneumatic Actuators With Stiffness Tuning¹

The inherent low stiffness in soft robots makes them preferable for working in close proximity to humans. However, having this low stiffness creates challenges when operating in terms of control and sensitivity to disturbances. To alleviate this issue, soft robots often have built-in stiffness tuning mechanisms that allow for controlled increases in stiffness. Additionally, redundant pneumatic manipulators can utilize antagonistic pressure to achieve identical positions under increased stiffness. In this paper, we develop a model to predict the stiffness and configuration of a pneumatic soft manipulator under different pressure inputs and external forces. The model is developed based on the physical characteristics of a soft manipulator while enabling efficient parameter estimation and computation. The efficacy of the modeling approach is supported via experimental results. [DOI: 10.1115/1.4064090]

Keywords: soft robotics, soft robotic manipulator, modeling, stiffness tuning, actuator, flexible structures, model validation, pneumatics

1 Introduction

Soft robotic manipulators can provide unique advantages over traditional rigid robots in terms of safety, flexibility, and degrees-of-freedom. This allows for new applications in areas such as human-robot collaboration and delicate handling of payloads. However, the low stiffness of soft robots creates potential issues as they are difficult to control, highly sensitive to external forces, and have limited payload capabilities. In order to counteract these challenges, soft robots can be equipped with stiffness tuning mechanisms [1]. There have been several methods reported for modeling and controlling soft robots that allow for simultaneous stiffness and position control. Antagonistic pressures have been used with planar pneumatic manipulators to achieve stiffness control [2] along with other methods such as particle, layer, and fiber jamming. Additionally, models such as the piecewise-constant curvature (PCC) model are used to simplify the control and representation of soft robots in three dimensions [3]. While the piecewise-constant curvature assumption allows for efficient implementation in, for example, path planning [4] and tracking control [5], in reality, this assumption often fails due to loading and other

While pneumatic systems have been developed to control soft robotic arms [6], the mappings between the controllable pressure inputs and the configuration outputs are dependent on the design of the manipulator and need to be captured in a model before they can be controlled. There has been work in tailoring the design and modeling of soft robots to meet specific requirements [7], but this model does not consider stiffness tuning. There have been methods for predicting the curvature of a beam under external tip forces [8,9], and the bending of inflatable beams is well understood [10]. Additionally, stiffness models have been presented for several types of soft manipulators including pneumatic artificial muscles [11] and fiber-reinforced elastomeric enclosures [12], but the redundancy to control the stiffness-independent positioning is lacking. Some soft robots have been developed with controllable skin stiffness that allows for both position and stiffness control [13] and the effects of external forces have also been examined for the modeling of soft manipulators [14]. However, in both these works, the effects are evaluated only on a planar manipulator instead of three-dimensional manipulators. Some models represent the soft manipulator in terms of Cosserat beams strain parameterization [15]. Due to their greater computational complexity, these models can be difficult to use in real-time feedback control.

Data-driven methods have also been used to model and control soft robotic manipulators, examples of which include Bayesian networks for reducing noise from model uncertainties [16] and neural networks for predicting the performance of soft manipulators [17], as well as Koopman-based models [18], which have further been integrated with an estimator for external load sensing and control

¹Paper presented at the 2023 Modeling, Estimation, and Control Conference (MECC 2023), Lake Tahoe, NV, Oct. 2–5. Paper No. MECC2023-153.
²Corresponding author.

Manuscript received July 24, 2023; final manuscript received November 3, 2023; published online December 8, 2023. Assoc. Editor: Peter H. Meckl.

[19]. However, these data-driven models often require large data sets for training and are vulnerable to overfitting.

In this paper, a novel semi-physical model for predicting the stiffness and position of a three-dimensional pneumatic soft manipulator is presented. The proposed modeling approach aims to combine the benefits of physics-based modeling and data-driven modeling, so that the resulting model carries physical interpretation while being computationally efficient. It works by estimating the stiffness and moments generated by actuation of the soft manipulator to calculate the resulting shape and position of the robot. In addition, the model allows for the easy incorporation of external forces such as gravity and payloads while maintaining a generality that can be applied to other continuum soft robots, specifically those with uniform shape and bending actuation.

The contents of this paper are organized as follows. First, in Sec. 2, the model is developed by considering how the length, stiffness, and internal moment can be calculated from the control input, as well as how external forces can be incorporated. The fabrication of a soft pneumatic manipulator and the experimental setup for model validation are described in Sec. 3. In Sec. 4, experimental results supporting the modeling approach are presented. Finally, concluding remarks along with a discussion of future work are provided in Sec. 5.

2 Modeling

2.1 Kinematic Background. A basic kinematic background of soft robots is required to formulate and apply the presented model. A core component of these kinematics is the PCC model, which is commonly used for soft robots as it describes a simplified bending shape prevalent with soft manipulators [3]. A summary of the necessary key concepts is given below.

In a piecewise-constant curvature model, the robot is divided into several segments each with uniform bending. Each segment can be described by its length L, bending angle θ , and bending direction φ . The shape of this segment is represented as an arc of a circle with curvature k

$$k = \frac{d^2w}{dx^2} = \frac{1}{r} = \frac{\theta}{L} \tag{1}$$

where w represents the deflection with respect to the length of the beam x, and r is the radius formed by the arc. By assuming that the curvature remains constant throughout the segment, it becomes easier to represent and reconstruct the shape of the segment based on only the three parameters. Without the PCC assumption, it is still possible to reconstruct the shape of the manipulator if the curvature is known at every point along the length of the manipulator. Let s be the arclength parameter of the manipulator, the curvature k(s) induced at a certain point s by an external moment M(s) is as follows:

$$k(s) = \frac{M(s)}{FI}, s \in [0, L]$$
 (2)

where E is the Young's modulus of the material, and I is the second moment of area of the segment. From Eq. (2), if the moment and physical properties do not change with respect to the length of the manipulator, the curvature would remain constant. However, this is not an exact representation as external forces such as gravity or a payload will induce additional (non-uniform) moment, causing it to bend at a non-constant curvature. In this paper, the following assumptions are made about the performance of the manipulator to make use of the PCC model without ignoring external forces:

- (1) The moment generated by the (internal) actuation of the soft manipulator, such as the pneumatic actuation, will be uniform with respect to the length of the manipulator at equilibrium. Any additional moment generated by external forces can be added to this value.
- (2) E and I do not vary along the length of the manipulator.

2.2 Modeling of Length Change. The first quantity we consider that is affected by the input pressures is the length of the pneumatic manipulator. The internal pressure produces force on all sides of the air chamber. While any expansion due to pneumatic pressures on the external and internal walls of soft manipulators is often constrained by the features of the soft arm such as fiber reinforcement, the top and/or bottom ends of the manipulator generally are not. The forces on the top and bottom of the manipulator from the pressures in the internal air chambers not only affect the overall length, but also drive the bending when such forces result in a difference in length with respect to the circumference.

The change in the length with respect to the circumference is a function of the input pressures. Ideally, the internal chambers of the soft manipulator would have identical effects under the same actuation pressure. However, due to the variance in the fabrication process, this is generally not the case, which is accommodated in the proposed model.

The change in length $\Delta L(\alpha)$ at a certain angle α around the circumference can be modeled as

$$\Delta L(\alpha) = P_1[a_1 + a_2 + (a_1 - a_2)\cos(\alpha)] + P_2\left[a_3 + a_4 + (a_3 - a_4)\cos\left(\alpha + \frac{2\pi}{3}\right)\right] + P_3\left[a_5 + a_6 + (a_5 - a_6)\cos\left(\alpha - \frac{2\pi}{3}\right)\right]$$
(3)

where P_1 , P_2 , and P_3 are the pressures in the three air chambers, shown in Fig. 1 and a_1-a_6 are physical constants describing the change in length per unit input pressure at certain points around the circumference. a_1 describes the change in length of the location closest to chamber one per unit pressure, and a_2 describes the change in length at the location opposite chamber one. a_3-a_6 are the counterparts for chambers two and three. These variables could be expanded to any number of chambers for a specifically designed soft robot as long as the angles between them are included in the cosine function term (e.g., the separation is 120 deg for the case of three chambers).

The overall length of the manipulator is usually described in terms of the length of the center of the manipulator, i.e., along the longitudinal axis. This axis will be perpendicular to the direction of bending. Therefore, if the direction of bending is found, the bending moment axis can be found and the length at this angle

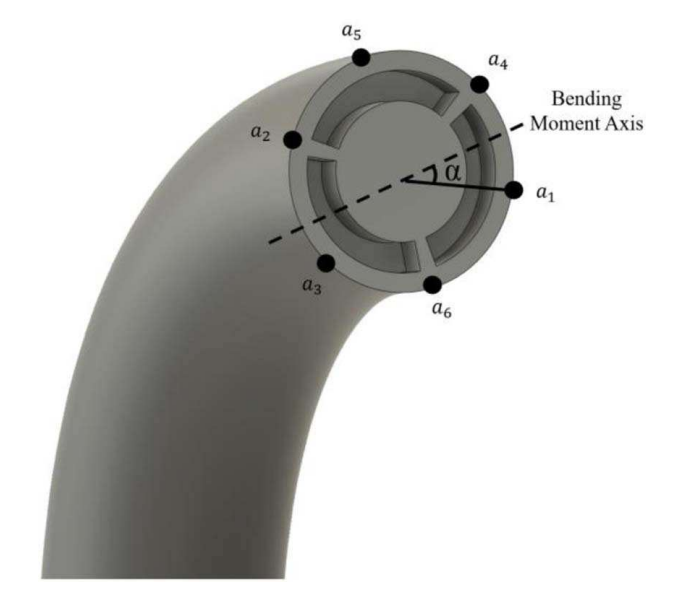


Fig. 1 Illustration of length positions around the circumference for a three-chamber pneumatic manipulator

will be equivalent to the length of the center of the manipulator. The length is the shortest on the innermost section of the manipulator and the longest on the outermost section. If the minimum or maximum of the length with respect to the angle is found, then it is known to either be the direction of bending or its opposite. If this value is then offset by 90 deg, the axis can be found. The maximum or minimum can be found by setting the derivative of the change in length with respect to the angle equal to zero in the following equation:

$$\frac{d\Delta L}{d\alpha} = -P_1(a_1 - a_2)\sin(\alpha) - P_2(a_3 - a_4)\sin\left(\alpha + \frac{2\pi}{3}\right)$$
$$-P_3(a_5 - a_6)\sin\left(\alpha - \frac{2\pi}{3}\right) = A * \sin(\alpha + \beta) \tag{4}$$

$$\beta = \tan^{-1} \left(\frac{P_2(a_3 - a_4) \frac{\sqrt{3}}{2} - P_3(a_5 - a_6) \frac{\sqrt{3}}{2}}{P_1(a_1 - a_2) - \frac{1}{2} P_2(a_3 - a_4) - \frac{1}{2} P_3(a_5 - a_6)} \right)$$
 (5)

which will be equal to zero when $\alpha = -\beta$. The location of the bending moment axis is thus equal to $-\beta + \frac{\pi}{2}$. The overall length of the manipulator at the center, L_c , can then be calculated as follows with the base length of the center of the manipulator under no pressure represented as L_0 :

$$L_c = L_0 + \Delta L \left(-\beta + \frac{\pi}{2} \right) \tag{6}$$

2.3 Modeling of Stiffness. Pneumatic particle jamming is one of the most popular stiffness tuning mechanisms and thus considered in this work, as illustrated in Fig. 2.

The bending stiffness of the manipulator EI has three main components that are dependent on the state of the robot. First, the soft manipulator has a base stiffness $EI_{\rm base} = b_1$ when no control inputs are activated. Additionally, according to Ref. [2], a higher stiffness is achieved by increasing the antagonistic forces between the inflated air chambers. The stiffness of a planar soft manipulator is proportional to the minimum pressure between its two antagonistic chambers. Therefore, a reasonable assumption is made that the increased stiffness of the manipulator is linearly related to the minimum pressure among three air chambers, which can be formulated as

$$EI_{\text{inflated}} = b_2 \min (P_1, P_2, P_3) \tag{7}$$

where b_2 is the constant gain. Lastly, the stiffness of the particle jamming mechanism changes linearly with the differential pressure

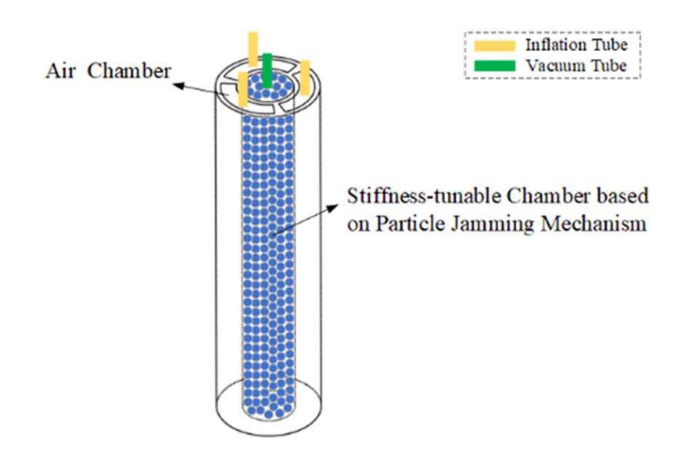


Fig. 2 Soft manipulator with particle jamming mechanism. Three inflation tubes control the bending motion, and the vacuum tube is used to jam the particle to increase the stiffness.

between the pressures in the air chambers and the stiffness tuning mechanism [20,21]. Specifically, the increased stiffness of the particle jamming mechanism EI_{particle} can be modeled as a linear function of the vacuum pressure V. Additionally, the actuated exterior air chambers also apply additional pressure to the stiffness tuning mechanism at the center of the manipulator. Consequently, EI_{particle} can be modeled as follows:

$$EI_{\text{particle}} = b_3 \left(V + \frac{1}{3} (P_1 + P_2 + P_3) \right)$$
 (8)

where b_3 is a constant.

In summary, the overall stiffness can be obtained as

$$EI = EI_{\text{base}} + EI_{\text{inflated}} + EI_{\text{particle}} = b_1 + b_2 \min(P_1, P_2, P_3) + b_3 \left(V + \frac{1}{3}(P_1 + P_2 + P_3)\right)$$
(9)

2.4 Modeling of Actuation Moment. The overall actuation moment experienced by the soft robotic arm can also be modeled as a function of the input pressures. The moment will have a magnitude and direction that will determine the magnitude and direction of bending. For the direction, $\varphi=0$ can be arbitrarily assigned to the bending angle when only chamber 1 is actuated. The resulting moments generated by all chambers can be broken down into component vectors and added together. As with the length, the overall magnitude of the moment generated by each chamber is not assumed to be identical and can be multiplied by a constant to better conform to the realized bending. The moment created by the air chamber pressures is equal to

$$M_x = c_1 P_1 + c_2 \cos\left(\frac{2\pi}{3}\right) P_2 + c_3 \cos\left(\frac{-2\pi}{3}\right) P_3 \tag{10}$$

$$M_y = c_2 \sin\left(\frac{2\pi}{3}\right) P_2 - c_3 \sin\left(\frac{-2\pi}{3}\right) P_3$$
 (11)

$$|M| = \sqrt{M_x^2 + M_y^2} \tag{12}$$

$$\angle M = \tan^{-1} \left(M_{\nu} / M_{\nu} \right) = \varphi \tag{13}$$

where $c_1 - c_3$ are constants that can be found from experiments that relate the moment generated by a specific chamber to its pressure. This equation can also be expanded to different air chamber layouts similar to the length. With a combination of the length, stiffness, and moment, the shape of the manipulator can be reconstructed based on the constant curvature model.

2.5 Effect of External Forces. The PCC assumption can be used with the previously defined parameters to derive the shape of the manipulator under actuation, but with external forces it does not hold. The effects of two common types of forces are described here. The first is a uniform load on the manipulator from its own weight. The second force is that of a point load on the manipulator.

A uniform load will create a varying moment along the manipulator. The load caused by the weight of the manipulator will have an overall force equal to the weight of the robot, W. This will create a uniform load with a force distribution of W/L_c . This force will always be directed straight down, so its contribution to the bending moment will vary with the orientation at that specific point. Assuming that the manipulator is pointing straight upwards at s=0, the moment along the length of the manipulator from gravity is equivalent to

$$M(s) = \int_{s}^{L_c} \frac{W}{L_c} \sin(\theta(s)) [x(L_c) - x(s)] ds$$
 (14)

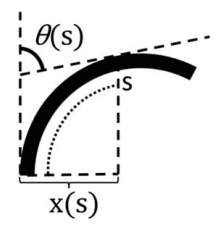


Fig. 3 Diagram of x(s) and $\theta(s)$

$$\theta(s) = \int_{0}^{s} k(s)ds \tag{15}$$

$$x(s) = \int_0^s \sin(\theta(s))ds \tag{16}$$

where $\theta(s)$ is the overall bending at the point and x(s) is the distance parallel from the ground to the point as shown in Fig. 3.

Assuming an initial constant bending from the pneumatic pressure, the moment due to gravity can be iteratively calculated and incorporated into the model.

Many interactions on the soft manipulator can be modeled as a point load: for example, a payload carried by the robot. A force of magnitude F with an angle of φ to the direction of bending applied at s=d on the manipulator will create moments along the length of the manipulator equal to

$$M(s) = F\sin(\theta(d))[x(d) - x(s)]\cos(\varphi), s \le d \tag{17}$$

3 Fabrication and Experimental Setup

3.1 Fabrication. This section covers the design and fabrication of a soft robotic arm for illustration and validation of the proposed modeling approach. The soft robot was created using silicone Dragon Skin 20 by Smooth-On. The length of the soft arm was 20 cm with a diameter of 42 mm. At the center of the soft arm was a hollow cylinder to allow a stiffness tuning mechanism to be added. The body of the soft arm contains three internal air chambers separated by 120 deg completely sealed by the silicone. The soft arm was fabricated through casting. The internal chambers of the arm were created using wax inserts. The wax was removed via melting in an oven and then the silicone was submerged in boiling water to remove any left-over wax. Holes from the casting were then either used to feed in air tubes or sealed with a silicone adhesive. The pneumatic air tubes were selected as 70 A silicone based on the adhesion strength documented in Ref. [22] which provided much stronger bonds and better sealing than polyethylene tubing. The arm was wrapped with inextensible Kevlar thread and adhered with an additional small coat of silicone to prevent bellowing of the air chambers when inflated. Computeraided design (CAD) designs of the robot are shown in Fig. 4.

At the center of the soft manipulator is a stiffness tuning mechanism that fills the hollow interior and prevents the expansion of the air chambers inwards. The mechanism was composed of a flexible exterior plastic casing enveloping some granular material.

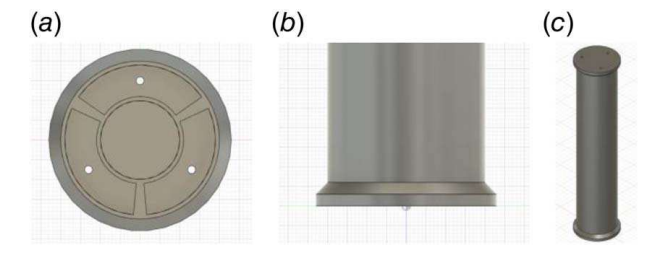


Fig. 4 CAD design of soft arm: (a) cross section of inside, (b) base of soft arm, and (c) ISO view of arm

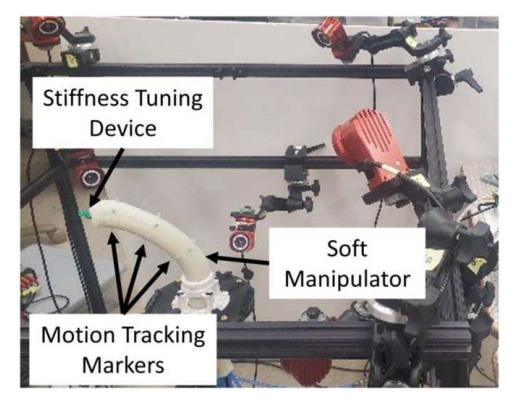


Fig. 5 Experimental setup

Examples of these materials include coffee grounds and beads. For this specific mechanism, 6 mm plastic beads were utilized. For the fabrication process, the plastic casing was enclosed via a heat press sealing the internal granular material with a pneumatic tube attached. The very end of the green casing of the particle jamming mechanism can be seen in Fig. 5.

3.2 Experimental Setup. The soft arm was controlled via pneumatic air pressure applied to the three internal air chambers. A proportional–integral–derivative (PID) controller and pressure sensors were used to regulate the air pressures to set values. For the following experiments, a maximum of 50 kPa pressure was utilized for any individual chamber to reduce the risk of damaging the soft arm, and this pressure also proved sufficient to provide bending of 90 deg as shown in Fig. 5. The vacuum pressure to the stiffness tuning chamber was generated with an external vacuum pump that can achieve up to 60 kPa of vacuum pressure.

For data acquisition, an OptiTrack motion capture system was utilized for measurement of the position of the manipulator. A set of ten cameras were used to track reflective markers placed on the soft arm. The markers captured by the motion tracking system arm are shown in Fig. 5. The markers were placed in sets of six separated by 60 deg around the circumference of the manipulator aligned with the geometry of the air chambers. Four sets of three markers were positioned from the base to the tip of the manipulator. The set at the base of the manipulator was attached to a 3D-printed part that is used to mount the robot to a table. These markers thus do not move and are utilized to locate the base position and orientation of the manipulator while the set of markers on the end are used for the tip position and orientation.

4 Results

4.1 Model Fitting Data. An initial set of data were gathered to identify and validate the model parameters $a_1 - a_6$, $b_1 - b_3$, and $c_1 - c_3$, which are shown in Table 1. These data consist of 30 sets of control inputs for the three chambers randomly generated between 10 kPa and 50 kPa. Additionally, each input to the

Table 1 Identified model parameters

a_1	0.658 mm/kPa	a_2 0 mm/kPa	
a_3	0.275 mm/kPa	$a_4 = 0.130 \text{ mm/kPa}$	
a_5	1.25 mm/kPa	$a_6 = 0.232 \text{ mm/kPa}$	
b_1	0.027 Nm ² /rad	Base stiffness	
b_2	$0.0003 \text{ Nm}^2/(\text{rad} \cdot \text{kPa})$	Air pressure stiffness	
b_3	$0.0013 \text{ Nm}^2/(\text{rad} \cdot \text{kPa})$	Vacuum stiffness tuning	
c_1	0.0061 Nm/kPa	Chamber 1 moment	
c_2	0.0078 Nm/kPa	Chamber 2 moment	
c_3	0.0065 Nm/kPa	Chamber 3 moment	

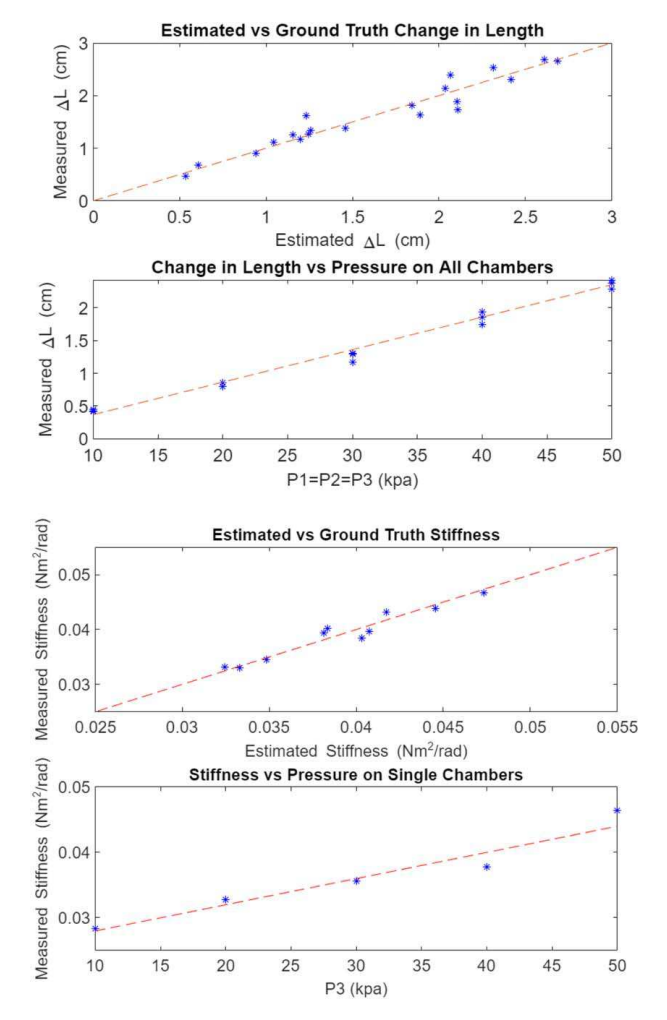


Fig. 6 Results of parameter matching: (top) plots of changes in length, and (bottom) plots of stiffness of the manipulator showing model efficacy and linearity

Table 2 Results of model shape prediction

	Absolute (cm)	Percent
Mean error	0.85	4.49%
Median error	0.5	2.63%
Maximum error	3.1	16.3%
Minimum error	0.13	0.68%

chambers had a 30% chance of being zero to allow for combinations of only one or two chambers to be inflated. The stiffness tuning chamber had a 50% chance to be on or off. Each data set was also accompanied with a corresponding measurement under a payload to calculate the stiffness. The first set of 20 data points was used to identify parameters for the model to see if it could work with a smaller sample size. The remaining ten data points were used to validate the model and not used to train the model.

Overall, three ground truth values needed to be measured to create the model: the length of the manipulator, the bending angle of the manipulator, and the stiffness of the manipulator. The length and bending angle can be calculated using the location of the markers. The centroid of the three base and tip markers was utilized to calculate the constant curvature value that creates the displacement between the two. The stiffness cannot be directly measured from a single set of data points. Instead, an analog force sensor was



Fig. 7 Reconstructed (center line) and measured (stars) shape under a new payload

used to apply a set amount of force to the tip of the manipulator perpendicular to its bending angle. The change in bending angle from before and after the force was applied is used to calculate the stiffness using Eqs. (2) and (17).

The data were then used to create a best-fit model by minimizing the two-norm of the error between the ground truth values and the model predicted values. The manipulator weighed 176 g and the effects of this weight were accounted for using Eq. (16). Comparisons of the measured ground truth and mode predictions for the length and stiffness are given in Fig. 6.

From the motion capture system, three points along the arm were used as ground truth values, and the average distance between these points and the model was used to calculate the error of the model. The resulting errors of the measured versus model positions from the ten data points the model was not trained on are shown in Table 2, with a representation of a modeled shape under a payload of 200 g shown in Fig. 7.

The results of these tests show the efficacy of the modeling approach. The model was able to produce a very low error for a soft robot, especially for one trained on only 20 data points. Additionally, the measured attributes of the soft manipulator being the length and stiffness had little error and showcased the linearity present in the model.

5 Conclusion

In this paper, a model for 3D pneumatic soft manipulators was developed that allows for the prediction of the position and stiffness of the manipulator. This model was experimentally validated with a fabricated soft robotic arm. The model, trained with only a small set of training data, was able to predict the shape and stiffness of the robot for a variety of random control inputs. Future work involves the extension of the modeling approach to the case of multi-segment manipulators. It is also of interest to extend the model to include the dynamic effects and examine its use for the design of feedback controllers.

Acknowledgment

This work was supported in part by the National Science Foundation (ECCS 2024649).

Conflict of Interest

There are no conflicts of interest.

Data Availability Statement

The datasets generated and supporting the findings of this article are obtainable from the corresponding author upon reasonable request.

References

- Park, W., Lee, D., and Bae, J., 2022, "A Hybrid Jamming Structure Combining Granules and a Chain Structure for Robotic Applications," Soft Rob., 9(4), pp. 669-679
- [2] Gillespie, M. T., Best, C. M., and Killpack, M. D., 2016, "Simultaneous Position and Stiffness Control for an Inflatable Soft Robot," 2016 IEEE International Conference on Robotics and Automation (ICRA), Stockholm, Sweden, May 16–21, pp. 1095–1101.
- [3] Webster, R. J., and Jones, B. A., 2010, "Design and Kinematic Modeling of Constant Curvature Continuum Robots: A Review," Int. J. Rob. Res., 29(13), pp. 1661–1683.
- [4] Fairchild, P. R., Srivastava, V., and Tan, X., 2021, "Efficient Path Planning of Soft Robotic Arms in the Presence of Obstacles," Modeling, Estimation and Control Conference, Austin, TX, Oct. 24–27, pp. 586–591.
- [5] Mei, Y., Fairchild, P., Srivastava, V., Cao, C., and Tan, X., 2023, "Simultaneous Motion and Stiffness Control for Soft Pneumatic Manipulators Based on a Lagrangian-Based Dynamic Model," American Control Conference (ACC), San Diego, CA, May 31–June 2, pp. 145–152.
- [6] Zhang, B., Chen, J., Ma, X., Wu, Y., Zhang, X., and Liao, H., 2022, "Pneumatic System Capable of Supplying Programmable Pressure States for Soft Robots," Soft Rob., 9(5), pp. 1001–1013.
- [7] Kan, Z., Pang, C., Zhang, Y., Yang, Y., and Wang, M. Y., 2022, "Soft Actuator With Programmable Design: Modeling, Prototyping, and Applications," Soft Rob., 9(5), pp. 907–925.
- [8] Lau, J. H., 1993, "Closed-Form Solutions for the Large Deflections of Curved Optical Glass Fibers Under Combined Loads," ASME J. Electron. Packag., 115(3), pp. 337–339.
- [9] Nallathambi, A. K., Lakshmana Rao, C., and Srinivasan, S. M., 2010, "Large Deflection of Constant Curvature Cantilever Beam Under Follower Load," Int. J. Mech. Sci., 52(3), pp. 440–445.
- [10] Veldman, S. L., Bergsma, O. K., and Beukers, A., 2005, "Bending of Anisotropic Inflated Cylindrical Beams," Thin-Walled Struct., 43(3), pp. 461–475.
- [11] Doumit, M., and Leclair, J., 2017, "Development and Testing of Stiffness Model for Pneumatic Artificial Muscle," Int. J. Mech. Sci., 120(1), pp. 30–41.

- [12] Bishop-Moser, J., Krishnan, G., and Kota, S., 2013, "Force and Moment Generation of Fiber-Reinforced Pneumatic Soft Actuators," IEEE/RSJ International Conference on Intelligent Robots and Systems, Tokyo, Japan, Nov. 3–7, pp. 4460–4465.
- [13] Chellattoan, R., and Lubineau, G., 2022, "A Stretchable Fiber With Tunable Stiffness for Programmable Shape Change of Soft Robots," Soft Rob., 9(6), pp. 1052–1061.
- [14] Ghalati, M. H. N., Ghafarirad, H., Suratgar, A. A., Zareinejad, M., and Ahmadi-Pajouh, M. A., 2022, "Static Modeling of Soft Reinforced Bending Actuator Considering External Force Constraints," Soft Rob., 9(4), pp. 778–787.
- [15] Boyer, F., Lebastard, V., Candelier, F., and Renda, F., 2021, "Dynamics of Continuum and Soft Robots: A Strain Parameterization Based Approach," IEEE Trans. Rob., 37(3), pp. 847–863.
- [16] Kim, D., Park, M., and Park, Y.-L., 2021, "Probabilistic Modeling and Bayesian Filtering for Improved State Estimation for Soft Robots," IEEE Trans. Rob., 37(5), pp. 1728–1741.
- [17] Loo, J. Y., Ding, Z. Y., Baskaran, V. M., Nurzaman, S. G., and Tan, C. P., 2022, "Robust Multimodal Indirect Sensing for Soft Robots Via Neural Network-Aided Filter-Based Estimation," Soft Rob., 9(3), pp. 591–612.
- [18] Bruder, D., Gillespie, B., Remy, D. C., and Vasudevan, R., 2019, "Modeling and Control of Soft Robots Using the Koopman Operator and Model Predictive Control," Robotics: Science and Systems, Freiburg im Breisgau, Germany, June 22–26.
- [19] Bruder, D., Fu, X., Gillespie, B. R., Remy, D. C., and Vasudevan, R., 2021, "Koopman-Based Control of a Soft Continuum Manipulator Under Variable Loading Conditions," IEEE Rob. Autom. Lett., 6(4), pp. 6852–6859.
- [20] Jiang, P., Yang, Y., Chen, M. Z. Q., and Chen, Y., 2019, "A Variable Stiffness Gripper Based on Differential Drive Particle Jamming," Bioinspir. Biomim., 14(3), p. 036009.
- [21] Li, Y., Chen, Y., Yang, Y., and Wei, Y., 2017, "Passive Particle Jamming and Its Stiffening of Soft Robotic Grippers," IEEE Trans. Rob., 33(2), pp. 446–455.
- [22] Bell, M. A., Becker, K. P., and Wood, R. J., 2022, "Injection Molding of Soft Robots," Adv. Mater. Technol., 7(1), p. 2100605.